Applied Catalysis B: Environmental 162 (2015) 260–267

Contents lists available at ScienceDirect

Applied Catalysis B: Environmental

journal homepage: www.elsevier.com/locate/apcatb

Nanostructured MnO_x catalysts in the liquid phase selective oxidation of benzyl alcohol with oxygen: Part I. Effects of Ce and Fe addition on structure and reactivity

Francesco Arena[a,b,*], Bianca Gumina[b], Agata F. Lombardo[a], Claudia Espro[a], Antonio Patti[c], Lorenzo Spadaro[b], Leone Spiccia[c]

[a] *Dipartimento di Ingegneria Elettronica, Chimica e Ingegneria Industriale, Università degli Studi di Messina, Viale F. Stagno D'Alcontres 31, I-98166 Messina, Italy*
[b] *Istituto CNR-ITAE "Nicola Giordano", Salita S. Lucia 5, I-98126 S. Lucia (Messina), Italy*
[c] *School of Chemistry and ARC Centre of Excellence for Electromaterials Science (ACES), Monash University, Clayton 3800, VIC, Australia*

ARTICLE INFO

Article history:
Received 5 May 2014
Received in revised form 23 June 2014
Accepted 26 June 2014
Available online 7 July 2014

Keywords:
MnO_x catalysts
Ce and Fe promoters
Selective oxidation
Benzyl alcohol
Structural-electronic effects

ABSTRACT

The effects of Ce (Ce_{at}/Mn_{at}, 0–1) and Fe addition ($(Ce_{at}+Fe_{at})/Mn_{at}$, 0.3) on the texture, structure and redox properties of MnO_x systems have been investigated. Irrespective of their loading, the Ce and Fe promoters lead to *nanostructured* composite systems with a much larger surface area than the oxide component alone. Both Ce and Fe ions improve catalyst reducibility because of structural effects enhancing the surface availability of high oxidation number Mn^{n+} ($n \geq 4$) sites. At variance with the inactivity of the CeO_2 and Fe_2O_3 promoters, the bare and promoted MnO_x catalysts drive the liquid phase oxidation of benzyl alcohol with oxygen in the range of 323–353 K with total aldehyde selectivity. The dependence of activity level on MnO_x loading and unchanging activation energy barrier (52 ± 5 kJ/mol) substantiate the lack of electronic effects attributable to both Ce and Fe promoters. Although a marked activity loss recorded after the 1st reaction cycle, calcination at $T \geq 473$ K fully restores the catalyst functionality.

1. Introduction

Benzaldehyde is an important fine chemical, finding extensive uses in the pharmaceutical, dyestuff, agrochemical and perfume industries, which is currently produced by the liquid phase hydrolysis of benzyl chloride or by the selective oxidation of toluene [1]; harmful reagents, complicated manufacturing steps, Cl-contamination and low product yields are yet severe drawbacks for environmental impact and process economics [1,2]. This stimulates a big research interest for new cleaner synthesis routes mostly based on the selective oxidation of benzyl alcohol [3–36]. Despite the fact that stoichiometric transition-metal reagents result in high product yields when applied in the oxidation of numerous alcoholic substrates, their use is restricted by costs and the co-generation of toxic waste that deserve special disposal treatments [4]. On the other hand, problems of corrosion, plating out on reactor walls, handling, recovery and reuse of the catalysts impede large-scale applications of homogeneous processes [2–4,30–36]. In fact, according to guidelines of *Green Chemistry*, the heterogeneous catalytic selective oxidation of benzyl alcohol with oxygen is the most environmentally and economically attractive option for benzaldehyde manufacture [2]. Supported noble-metal catalysts (*e.g.*, Pt, Pd, Au, Ru, Rh) display good performance under mild reaction conditions [5–15] but high costs and deactivation phenomena by *over-oxidation* and/or *fouling* of active sites hinder their industrial exploitation [3,37]. On the other hand, research on transition metal-oxide catalysts documents that bare and promoted MnO_x systems feature high activity and selectivity to benzaldehyde in the liquid phase oxidation of benzyl alcohol with oxygen in the range of 303–433 K; this has been attributed to a high redox functionality favoring an enhanced mobility of surface-oxygen species [3,4,14,20–29]. In this respect, several oxide promoters have been reported to improve the redox functionality of MnO_x materials in both gas and liquid phase catalytic reactions [38].

Therefore, this work is aimed at assessing the effects of Ce (Ce_{at}/Mn_{at}, 0–1) and Fe ($(Ce_{at}+Fe_{at})/Mn_{at}$, 0.3) addition on structure, redox properties and reactivity of MnO_x catalysts in the liquid phase selective oxidation of benzyl alcohol with oxygen (*T*,

* Corresponding author at: Dipartimento di Ingegneria Elettronica, Chimica e Ingegneria Industriale, Università degli Studi di Messina, I-98166 Messina, Italy. Tel.: +39 0906765606; fax: +39 090391518.
E-mail address: Francesco.Arena@unime.it (F. Arena).

http://dx.doi.org/10.1016/j.apcatb.2014.06.054
0926-3373/

Table 1
List and physico-chemical properties of the studied catalysts.

Catalyst	Chemical composition (wt%)[a]				Atomic ratio			SA (m^2/g)	PV (cm^3/g)	APD (nm)
	MnO_x	CeO_x	FeO_x	KO_x	(Ce/Mn)	(Fe/Mn)	(K/Mn)			
M1C1	34.4	65.3	0.0	0.2	0.98	0.0	0.01	190	0.46	25
M3C1	59.9	36.9	0.0	3.3	0.31	0.0	0.10	184	0.57	27
M5C1	66.9	28.4	0.0	4.8	0.21	0.0	0.13	159	0.56	30
M9C1	77.0	17.6	0.0	5.4	0.11	0.0	0.13	136	0.49	31
M	93.5	0.0	0.0	6.5	0.0	0.0	0.13	94	0.34	31
C	0.0	100	0.0	0.0	0.0	0.0	0.0	128	0.10	3
F	0.0	0.0	100	0.0	0.0	0.0	0.0	33	0.10	15
M6C1F1	65.0	21.6	9.7	4.5	0.16	0.16	0.13	135	0.26	27
M3F1	74.6	0.0	20.9	4.7	0.0	0.31	0.12	136	0.38	27

[a] Expressed as MnO_2, CeO_2, Fe_2O_3 and K_2O.

323–363 K). A systematic analysis of activity data sheds lights onto the factors controlling the oxidation functionality of MnO_x catalysts, disclosing the lack of *electronic* effects in both Ce and Fe promoted systems.

2. Experimental

2.1. Catalysts preparation

Cerium (M_xC_y) and iron ($M_xC_yF_z$) promoted MnO_x catalysts with different atomic ratios (Mn/Ce/Fe, *x*/*y*/*z*) were prepared *via* a *redox-precipitation* route [39–41], according to the following procedure [41]. Deionized water (150 mL) at pH ≈ 4.5 (adjusted by HNO_3 addition) was heated at 343 K under stirring and nitrogen flow to remove oxygen. Then, appropriate amounts of the $Mn(NO_3)_2{\cdot}4H_2O$ (>97%, *Carlo Erba*) and $FeSO_4{\cdot}7H_2O$ (>99.5%, *Carlo Erba*) precursors were solubilized therein and titrated by the dropwise addition of an aqueous solution (0.2 L) of $KMnO_4$ (≥99%, *Carlo Erba*) and $Ce(NH_3)_2(NO_3)_6$ (>98.5%, *Aldrich*) precursors (pH ≈ 1). During titration, the pH of the solution was kept constant (4.5 ± 0.5) by addition of KOH solution (0.1 M), forcing the following *redox-precipitation* reactions

$$MnO_4^- + 3e^- + 2H_2O \rightarrow MnO_2\Downarrow + 4HO^- \quad (1)$$

$$Ce^{4+} + 2H_2O \rightarrow CeO_2\Downarrow + 4H^+ \quad (2)$$

$$Mn^{2+} + 2H_2O \rightarrow MnO_2\Downarrow + 4H^+ + 2e^- \quad (3)$$

$$2Fe^{2+} + 3H_2O \rightarrow Fe_2O_3\Downarrow + 6H^+ + 2e^-. \quad (4)$$

After titration, the solids were digested for 1 h, filtered, and repeatedly washed with hot distilled water, dried at 373 K (16 h) and further calcined in air at 673 K (6 h). Bare CeO_2 and Fe_2O_3 samples were prepared by the reflux method [42] and addition of Fe^{2+} precursor to a H_2O_2 solution (pH ≈ 4.5), respectively. The list of the catalysts with the relative code and main physico-chemical properties is given in Table 1.

2.2. Catalyst characterization

X-ray fluorescence (XRF) analyses were performed using a *Bruker AXS-S4 Explorer* spectrometer taking the $K\alpha_1$ transitions emission values of Mn (5.9 keV), Ce (4.8 keV) and Fe (6.4 keV) to determine the analytical composition of the catalysts.

N_2-physical adsorption isotherms (77 K) were obtained using an *ASAP 2010* static adsorption device (*Micromeritics Instrument*). Surface area (SA), pore volume (PV) and average diameter (APD) data were obtained from the elaboration of the isotherms by the standard BET and BJH methods, respectively.

X-ray diffraction (*XRD*) analyses were performed using a *Philips X-Pert* diffractometer, operating with Ni β-filtered Cu *K*α radiation (40 kV; 30 mA) at a scan rate of 0.05°/min.

Temperature programmed reduction (TPR) measurements in the range of 293–1073 K were carried out using a linear quartz microreactor (d_{int} = 4 mm) heated at the rate of 12 K/min. The reactor was loaded with a catalyst sample of *ca* 25 mg and fed with either 5% H_2/Ar (H_2–TPR) or 5% CO/He (CO–TPR) carriers (*F*, 60 stp mL/min). The consumption of H_2 and CO was monitored by a TCD, water and carbon dioxide being fully removed by a "chemical trap" containing $Mn(ClO_4)_2$ and ascarite, respectively.

2.3. Catalyst testing

A 3-necked pyrex glass flask reactor, equipped with a Hg-thermometer and a reflux condenser, was loaded with a suspension of 49 mL of toluene, 0.5 mL of ethyl benzoate as *internal standard* and 0.5 mL (4.8 mmol) of benzyl alcohol (*std conditions*). The reactor was heated at 343 K under vigorous stirring and oxygen flow (60 stp mL/min) adding, then, (t_0) 0.45 g of powdered catalyst sample (d_p < 200 μm). Constant conversion rates (±5%) at different catalyst and benzyl alcohol concentrations (w_{cat}/w_{Alc}, 0.9) confirmed the lack of significant external mass transfer resistances on reaction kinetics [37]. The reaction was monitored by withdrawing *ca* 0.1 mL samples from the reactor and analyzing them using a GC (*Agilent Technologies, GC System 7890A*) equipped with a capillary column (*Restek, Rxi-1ms*) connected to a FID detector. The reproducibility of conversion–concentration data was within ±5%.

3. Results and discussion

3.1. Textural and structural properties

Composition data in Table 1 show a good agreement between design and experimental Mn/Ce/Fe atomic ratios [39,41] and the presence of significant amounts of potassium in all the catalysts, despite a careful solid washing at the end of the synthesis process. In fact, the K content parallels the MnO_x loading, as documented by the asymptotic growth of the atomic K/Mn ratio from 0.01 to a maximum value of 0.12–0.13 (Fig. 1). Considering that the synthesis of the various catalysts implies an almost unchanging (0.4–0.5) Mn^{VII}/Mn^{II} molar ratio, the significant retention of K^+ ions could be a consequence of a strong "K–MnO_x" interaction, especially for Mn/promoter atomic ratios larger than 0.3 [26,27,43,44]. On the other hand, the addition of the promoters has a very positive impact on surface exposure as indicated by larger surface area (SA) values of the composite catalysts in comparison to bare oxides (Table 1). The positive structural effect of cerium is probed by the asymptotic SA increase with the Ce/Mn ratio (Fig. 2A) from *ca* 90 (M) to 190 m^2/g (M1C1) [45], although a comparable growth of pore volume (PV) mirrors minor changes in the average pore diameter (APD, 25–30 nm). Replacement of Ce with Fe ions (($Ce_{at} + Fe_{at}$)/Mn_{at}, 0.3) causes a drop in SA from 185 to 135 m^2/g, with no differences between M6C1F1 and M3F1 catalysts being observed (Fig. 2B).

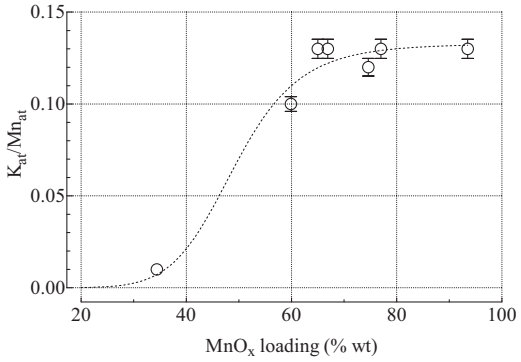

Fig. 1. Influence of the loading on the atomic K/Mn ratio of bare and promoted MnO_x catalysts.

Notably, also in this case a concomitant PV decrease (Table 1) reflects an unchanging APD (27 nm), indicating that catalyst composition affects the surface area without altering the intra-particle transport properties. In fact, a systematic decrease in both SA and PV with MnO_x loading could depend on a sort of "cement effect", perhaps enhanced by K^+ ions (Fig. 1), causing an incipient sticking of the catalyst grains.

Remarkable effects of Ce and Fe addition on the structure of the MnO_x phase are also evident from the XRD patterns, shown in Fig. 3. The bare M sample shows several peaks in the 2θ range of 10–80° attributable to sparse crystalline domains of the pyrolusite (JCPDS 24-735) and vernadite (JCPDS 15-604) phases, although

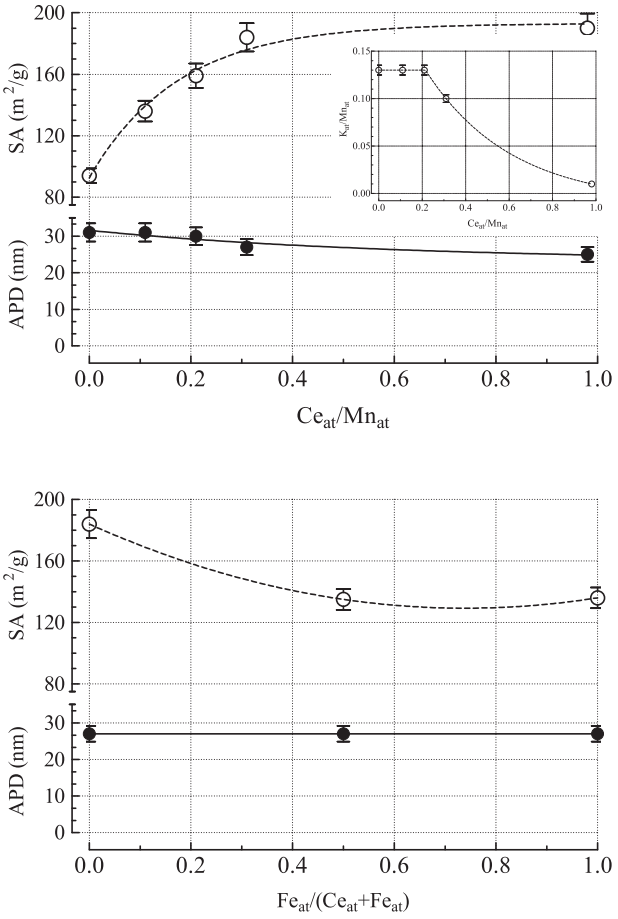

Fig. 2. (A) Influence of the atomic Ce/Mn ratio (x/y) on surface area (SA) and average pore diameter (APD) of M_xC_y catalysts; (B) Influence of the Ce and Fe content on SA and APD of the M3C1, M6C1F1 and M3F1 catalysts.

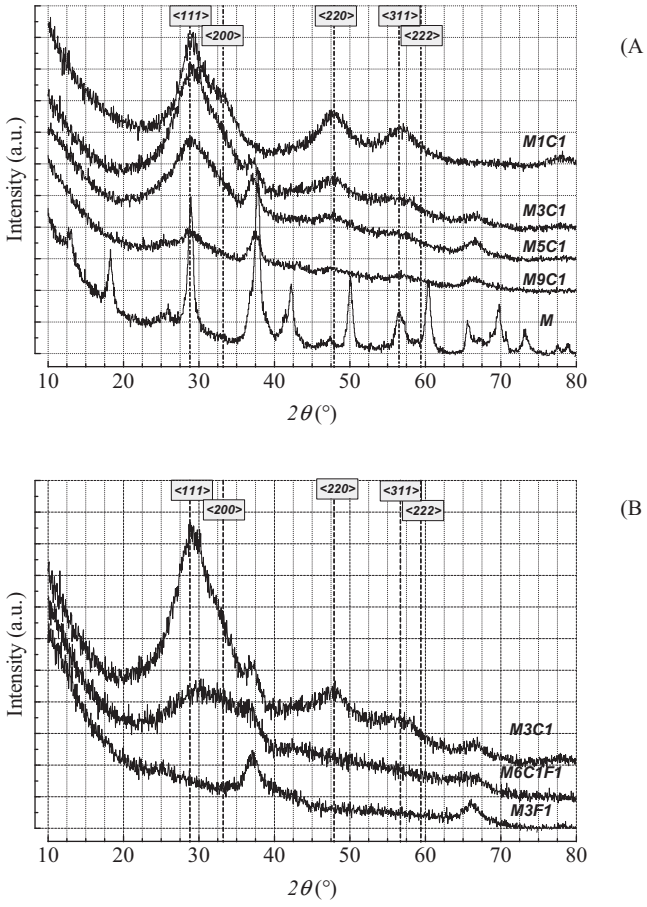

Fig. 3. XRD patterns of: (A) Ce-promoted catalysts; (B) M3C1, M6C1F1 and M3F1 catalysts. *For reference the position of the main reflections of the cerianite habit are indicated.*

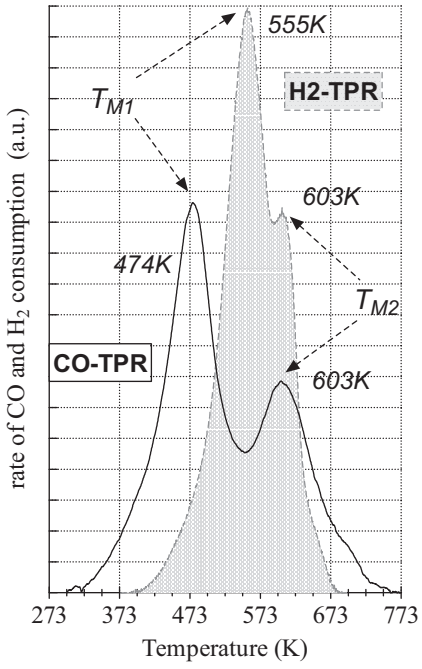

Fig. 4. H2–TPR and CO–TPR profiles of the M3C1 catalyst.

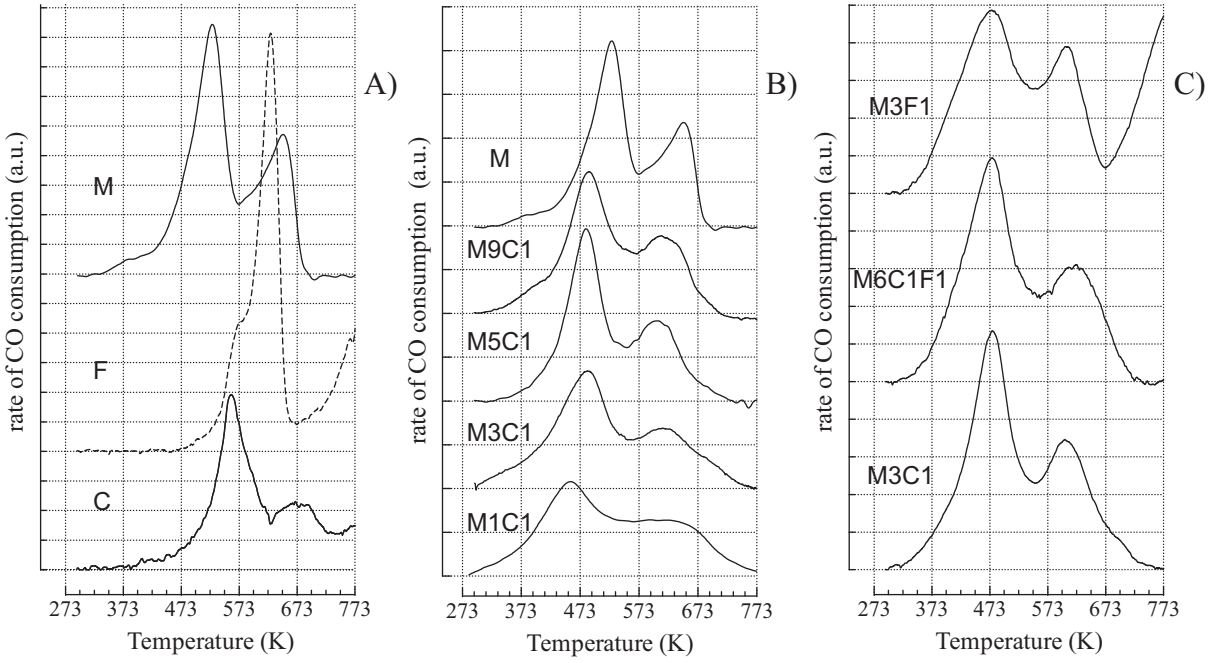

Fig. 5. CO–TPR profiles of: (A) bare C, F and M oxides; (B) Ce-promoted catalysts; and (C) M3C1, M6C1F1 and M3F1 catalysts (*profiles in (B) and (C) normalized to the MnO_x content*).

birnessite-like structures cannot be excluded [46]; the width and low intensity of diffraction peaks (*e.g.*, noise-to-signal ratio) are consistent with a rather small size and concentration of crystalline structures in the bare M system. All those diffraction lines are completely lost in the XRD patterns of Ce-promoted systems although small and broad reflections at *ca* 37 and 66.5° indicate some incipient crystallization of the active phase in the M3C1, M5C1 and M9C1 catalysts. In addition, the broad peak at *ca* 29° and the smaller peaks at *ca* 47 and 57° (Fig. 3A) indicate the presence of crystalline ceria nanoparticles in Ce-promoted catalysts (Fig. 2A) [39–41,45,47]. Accordingly, the replacement of Ce with Fe causes an evident decrease of such signals (Fig. 3B), while the comparable intensity and shape of the peaks at 37 and 66.5° indicate an incipient crystallization of the active phase also in the M6C1F1 and M3F1 catalysts despite MnO_x loadings higher than M3C1 sample (Table 1).

Overall, the fact that the addition of very low amounts of Ce and Fe ions hinders any "long-range" ordered MnO_x structures coupled to the similar structural characteristics of promoted catalysts (Fig. 2) confirm that the redox-precipitation synthesis route favours a quasi-molecular dispersion of MnO_x, CeO_x and FeO_x phases, irrespective of composition [39–41,45]. However, because of the presence of K^+ ions [22,27,43,44]; the similar diffraction patterns of the various MnO_x [27,43,44,48], CeO_2 [39–41,45] and Fe_2O_3 [48] phases; and the very small size of the oxide domains, the structure of bare and promoted MnO_x systems be more complex than ascertained from XRD analysis.

3.2. Redox pattern

We previously established that the structure, dispersion and oxide-interaction effects determine the reduction pattern of MnO_x catalysts [49], although this also depends on the intrinsic reactivity of the reducing species [50,51]. Therefore, a comparative TPR study using either H_2 (H_2–TPR) or CO (CO–TPR) was carried out first. In fact, the reduction profiles of the M3C1 catalyst in Fig. 4 show a marked downward shift of the CO–TPR pattern, explainable by the fact that the reducing action of H_2 molecules comes across a preliminary activation step that is the splitting of H—H bonds and the consequent generation of "reactive" atomic species. This accounts for the marked upward shift of both $T_{o,red}$ and T_{M1} under H_2, while the constant T_{M2} values (Fig. 4) rule out significant effects of the reducing molecule at $T > 473$ K. In fact, a lower mobility and accessibility of CO molecules across the catalyst structure (*i.e.*, *spillover*) explain the broader shape of the T_{M2} peak recorded by the CO–TPR measurement (Fig. 4). Apart from such peculiar differences linked to the reactivity of H_2 and CO, the H_2–TPR and CO–TPR profiles of the M3C1 catalyst essentially exhibit the same characteristics, with two main peaks accounting for reduction ($H_2/Mn \approx CO/Mn \approx 1$) of surface Mn^{IV} sites (T_{M1}) and MnO_x clusters (T_{M2}) to MnO [49].

Since CO–TPR analysis provides a more reliable overview of the catalysts reducibility in the temperature range of benzyl alcohol oxidation tests (323–363 K), the CO–TPR profiles of the studied catalysts are compared in Fig. 5, while $T_{o,red}$, T_{M1}, T_{M2}, and CO consumption data are summarized in Table 2. Among bare systems (Fig. 5A) manganese oxide (M) is the most reducible one with a $T_{o,red}$ of *ca* 335 K and two main peaks at *ca* 530 and 650 K accounting for

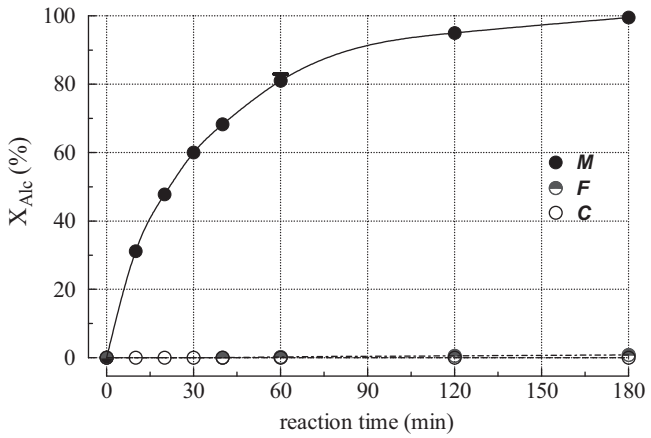

Fig. 6. Selective oxidation of benzyl alcohol on the bulk M, C and F systems: conversion *vs.* reaction time (*T, 343K; V, 50 mL; V_{Alc}, 0.5 mL (4.86 mmol); w_{cat}, 0.45 g; F_{O2}, 60 mL/min; P, 1 atm*).

Table 2
CO–TPR data of bare and promoted MnO_x catalysts.

Catalyst	$T_{o,red}$ (K)	T_{M1} (K)	T_{M2} (K)	CO consumption ($mmol/g_{cat}$)	CO/Mn
M1C1	280	452	616	3.60	0.92
M3C1	293	477	614	6.30	0.94
M5C1	300	482	615	6.70	0.87
M9C1	297	490	612	8.07	0.91
M	337	552	647	11.52	1.03
M6C1F1	303	476	629	6.84	0.92
M3F1	299	474	604	6.90[a]	0.80[a]

[a] In the range of 273–673 K (see Fig. 4C).

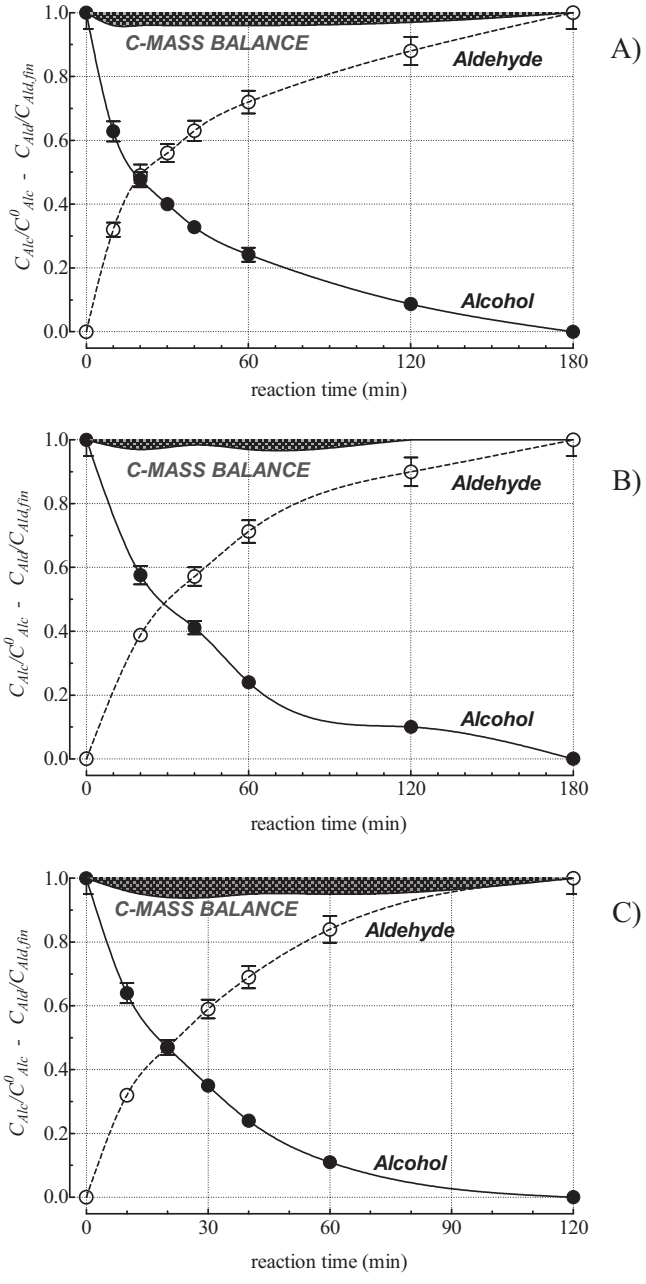

Fig. 7. Selective oxidation of benzyl alcohol on M (A), M3C1 (B) and M3F1 (C) catalysts: benzyl alcohol and benzaldehyde concentration and C mass-balance *vs.* reaction time *(T, 343K; V, 50 mL; V_{Alc}, 0.5 mL (4.86 mmol); w_{cat}, 0.45; F_{O2}, 60 mL/min; P, 1 atm).*

the stepwise reduction ($Mn^{IV} \rightarrow Mn^{III} \rightarrow Mn^{II}$) of MnO_2 *nanoparticles* to MnO (CO/Mn ≈ 1) [49]. The bulk C and F systems feature much higher $T_{o,red}$ values (Table 2) and one resolved peak centred at 550 and 630 K, accounting for an incipient reduction of surface Ce^{IV} and Fe^{III} ions, respectively.

The promoting effect that Ce has on the reducibility of the MnO_x phase (Fig. 5B) is evident from a systematic downward shift of the T_{M1} with the Ce/Mn ratio (Table 2), although minor $T_{o,red}$ variations (280–337 K) suggest that the higher reducibility depends mostly on structural effects of ceria promoter, enhancing the exposure of very reducible $Mn^{n+}(n \geq 4)$ sites. The intensity and sharpening of the T_{M2} peak mirror an increasing concentration of MnO_x clusters at lower Ce/Mn ratios (Fig. 5B), while the concomitant reduction of surface Ce^{IV} ions (Fig. 5A) accounts for the broad shape of the T_{M2} component, mostly in the M1C1 catalyst. Analogous $T_{o,red}$ and T_{M1} values (Table 2) disclose that a partial or total replacement of Ce with Fe ($Mn_{at}/(Ce_{at} + Fe_{at})$, 3) has no significant effects on catalyst reducibility at $T < 673$ K (Fig. 5C), while the subsequent CO consumption monitors the incipient reduction of Fe_2O_3 clusters (Fig. 5A) in the M3F1 catalyst. Normalized to the MnO_x content, the peaks area indicates small differences in CO consumption (CO/Mn, 0.9–1.0). Therefore, despite an incipient reduction of the CeO_2 and Fe_2O_3 phases hinders a definitive assessment of the Mn average oxidation number (AON), the CO–TPR features at $T < 473$ K indicate the prevailing presence of easily reducible Mn^{n+} $(n \geq 4)$ sites on both bare and promoted MnO_x catalysts [49].

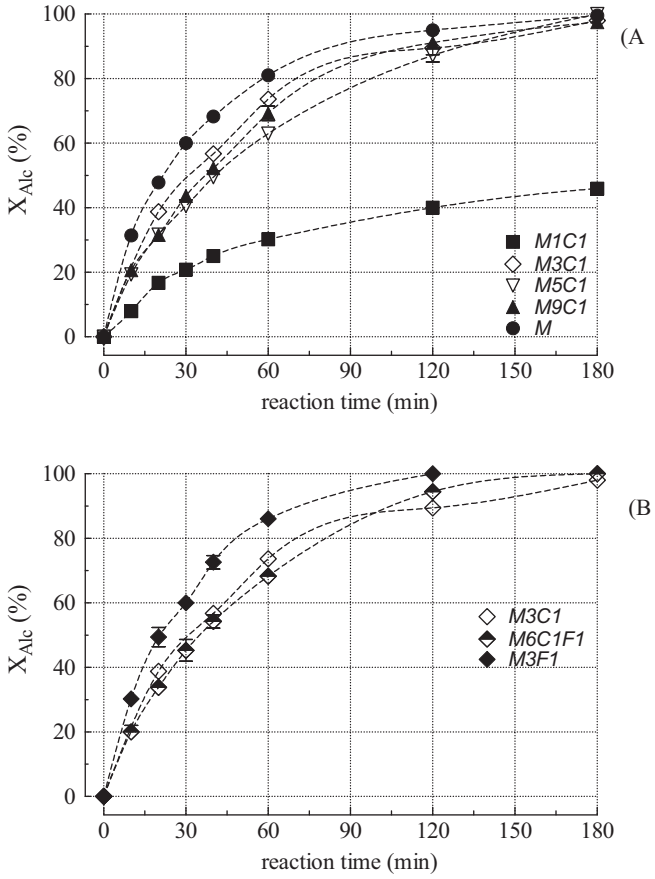

Fig. 8. Selective oxidation of benzyl alcohol on Ce (A) and Fe (B) promoted MnO_x catalysts: conversion *vs.* reaction time *(T, 343K; V, 50 mL; V_{Alc}, 0.5 mL (4.86 mmol); w_{cat}, 0.45 g; F_{O2}, 60 mL/min; P, 1 atm).*

3.3. Activity pattern

The reactivity of the bare MnO_x (M), CeO_2 (C) and Fe_2O_3 (F) systems in the selective oxidation of benzyl alcohol with oxygen is compared in Fig. 6. Both the C and F systems are not active under std reaction conditions (*T*, 343 K; w_{cat}/w_{Alc}, 0.9), while the MnO_x material exhibits a remarkable performance leading to a complete conversion of alcohol to benzaldehyde (*S* > 99%) in *ca* 3 h. Disclosing a direct relationship between activity and reducibility (*vide supra*), these results indicate that MnO_x plays the role of active phase [3,4,14,20–29] while minor would be the contribution of promoters to the functionality of composite catalysts [52,53].

The concentration profiles of benzyl alcohol and benzaldehyde of bulk and promoted (M3C1, M3F1) MnO_x catalysts (Fig. 7) depict similar specular exponential-like trends, resulting in a satisfactory C mass balance throughout reaction time (±5%). This discloses a minor influence of adsorption phenomena on alcohol conversion and also confirms that benzaldehyde is the sole reaction product. In fact, carrying out a benzaldehdye oxidation test on the M3C1 catalyst under std conditions a conversion lower than 5% was recorded after 5 h. This poor aldehyde oxidation functionality could be explained considering that the alcohol → aldehyde oxidation consists of an oxidative dehydrogenation

$$C_6H_5-CH_2OH + 1/2O_2 \rightarrow C_6H_5-CHO + H_2O, \quad (5)$$

at variance of the (consecutive) oxidation of benzaldehyde to benzoic acid

$$C_6H_5-CHO + 1/2O_2 \rightarrow C_6H_5-COOH, \quad (6)$$

which involves the insertion of oxygen onto C-atom of the carbonyl group [50]. Therefore, the high selectivity of MnO_x catalysts could depend on their poor ability to drive a nucleophilic oxidation of benzaldehyde. In turn, this infers that the active oxygen species for alcohol oxidation should be electrophilic rather than nucleophilic, according to the fact that either O_2^- [20] or O_2^{2-} [26] species have been claimed forming on OMS-2 type materials under comparable reaction conditions. A poor benzoic acid selectivity (<20%) in presence of H_2O_2 as oxidant [32,33] could support the thought that different mechanisms leads to aldehyde and acid.

Despite having no effects on selectivity, the promoters influence the reactivity of the MnO_x phase as shown in Fig. 8. In particular, among the Ce-based catalysts, M1C1 (Ce/Mn, 1) has the

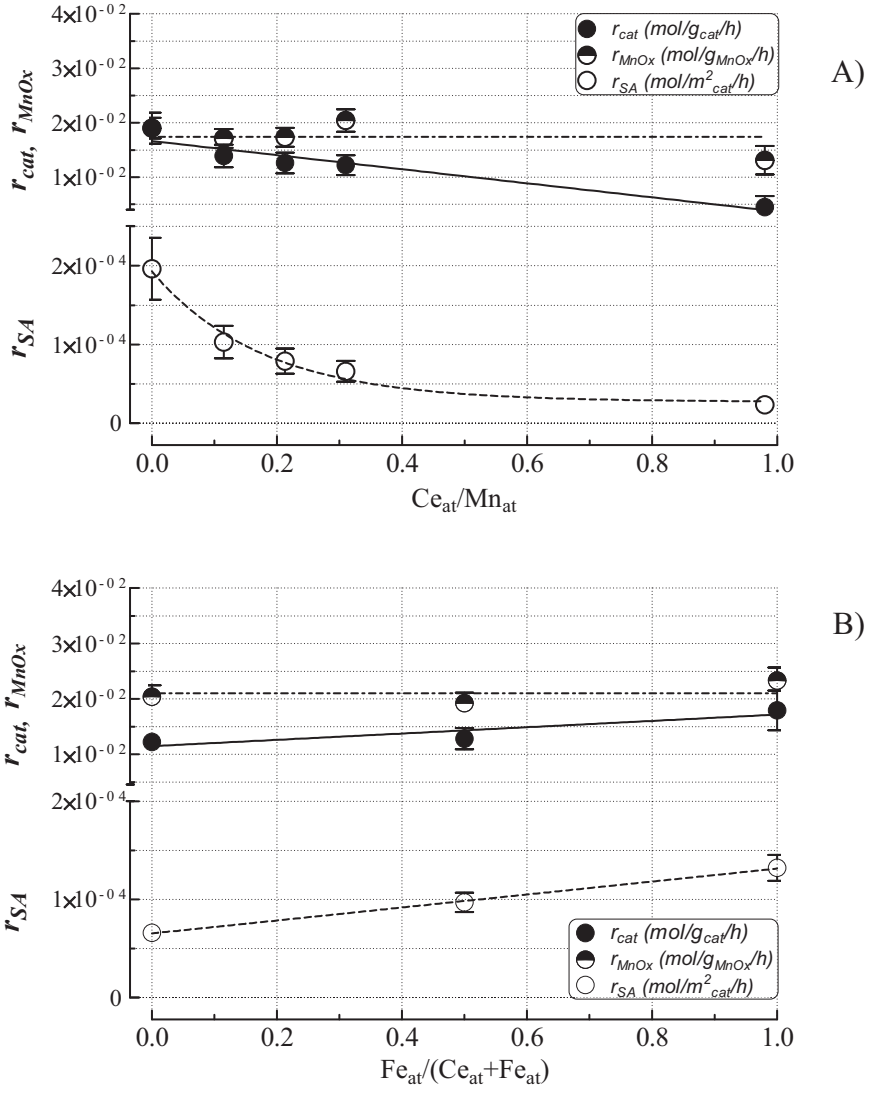

Fig. 9. Effect of the catalyst composition on the various specific initial rates: (A) influence of the Ce/Mn atomic ratio on the reactivity of Ce-promoted catalysts; and (B) influence of the Ce and Fe content on the reactivity of M3C1, M6C1F1 and M3F1 catalysts.

Table 3
Initial reaction rates in the selective oxidation of benzyl alcohol on M, M3C1 and M3F1 catalysts in the range of 333–363 K.

Catalyst	T (K)	r_{cat} (mol/g_{cat} h)	r_{MnO_x} (mol/(g_{MnO_x} h))	r_{SA} (mol/(m_{cat}^2 h))
M	333	8.6E – 03	8.6E – 03	9.0E – 05
	343	1.9E – 02	1.9E – 02	2.0E – 04
	363	4.3E – 02	4.3E – 02	4.6E – 04
M3C1	333	8.0E – 03	1.3E – 02	4.4E – 05
	343	1.5E – 02	2.4E – 02	7.9E – 05
	363	4.3E – 02	7.2E – 02	2.4E – 04
M3F1	333	1.2E – 02	1.6E – 02	9.0E – 05
	343	1.8E – 02	2.3E – 02	1.5E – 04
	353	3.5E – 02	4.5E – 02	2.6E – 04

lowest activity leading to a final (5 h) conversion value of only 50%, while the reactivity level of the M3C1, M5C1 and M9C1 samples (Ce/Mn < 0.3) compares to that of the bare system, ensuring a complete alcohol conversion in 3–4 h (Fig. 8A). Replacement of Ce with Fe has a positive effect on activity since both M6C1F1 and M3F1 catalysts show conversion rates higher than M3C1 catalyst (Fig. 8B).

In view of the lack of a formal kinetic law analysis, the specific catalytic activity was probed by the calculation of the initial reaction rates by the method of the tangent to the conversion curve for $X_{Alc} \rightarrow 0$. The effect of catalyst composition on the specific reaction rate *per* catalyst (r_{cat}) and MnO_x (r_{MnO_x}) weight and SA (r_{SA}) units are shown in Fig. 9. The reactivity of Ce-promoted systems decreases regularly with the Ce/Mn ratio (r_{cat}, 0.019–0.0045 mol/(g_{cat} h)), resulting in an exponential decay of the specific surface activity (r_{SA}, 2.0–0.2 E-04 mol/(m_{cat}^2/h)) also because of the SA increase (Fig. 2A). This substantiates an unprecedented negative effect of cerium on the oxidative functionality of the MnO_x system, although a fairly constant MnO_x rate rules out significant *electronic* effects of on the functionality of the active phase (Fig. 9A) [53].

The substitution of Ce with Fe has a positive influence on the reactivity of the M3C1 catalyst, as indicated by a specific rate increasing from *ca* 0.012 to 0.018 mol/g_{cat}/h (Fig. 9B). This accounts for a specific surface activity rising linearly with the Fe content, while a constant MnO_x rate (r_{MnO_x}, 0.019–0.023 mol/(g_{MnO_x} h)) indicates an unchanged functionality of the active phase; in fact, these trends mirror the higher MnO_x content of M6C1F1 and M3F1 catalysts than for the M3C1 sample (Table 1) suggesting the absence of significant chemical effects also in Fe-promoted catalysts. This was definitively ascertained by comparing the energetic barrier of benzyl alcohol oxidation on M, M3C1 and M3F1 catalysts from the initial reaction rate values in the range of 333–363 K listed in Table 3. For all the catalysts, the temperature dependence of the reaction rates provide fairly reliable Arrhenius plots, which on analysis gave analogous values of the activation energy barrier (E_{app}), namely between 52 and 57 kJ/mol (Fig. 10), that is diagnostic of an unchanging catalytic functionality due to a negligible, if any, influence of oxide promoters on the chemical (electronic) properties of the active MnO_x phase.

Furthermore, despite the general trends discussed earlier (Fig. 9), the M3C1 and M3F1 catalysts show similar slightly higher MnO_x reaction rates (Fig. 10) than the bulk M sample, probably because of the aforesaid structural effects of Ce and Fe promoters enhancing MnO_x dispersion and exposure and catalyst reducibility as well (*vide supra*). On the other hand, the Arrhenius plots in Fig. 10 show a reverse order in the specific surface activity, resulting higher for the bulk M than M3C1 and M3F1 catalysts; this depends on the negligible, if any, contribution of the surface CeO_2 and FeO_2 sites to the catalytic functionality of the composite systems. A slightly higher surface activity seems consistent with a higher MnO_x dispersion of the M3F1 sample than counterpart M3C1 one (Fig. 10). Then,

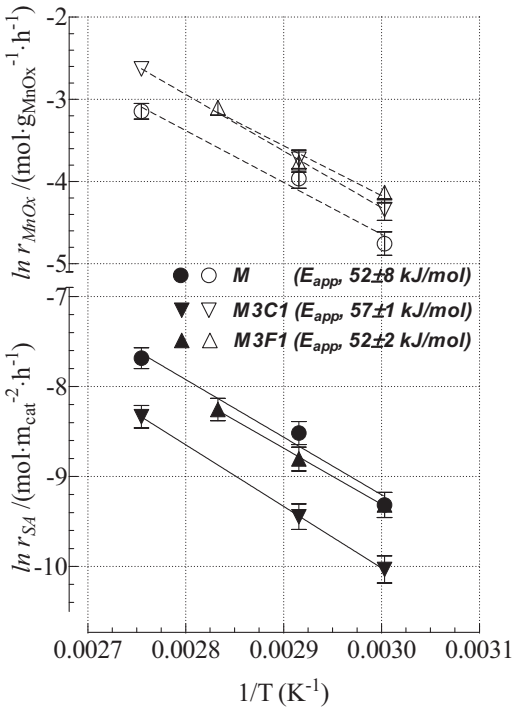

Fig. 10. Arrhenius plot of the initial specific reaction rates of the M, M3C1, and M3F1 catalysts in the range of 333–363 K.

despite the redox-precipitation synthesis route promoting the dispersion of the oxide and favouring the interaction of the various oxide phases in composite catalysts, the reactivity data are consistent with the lack of electronic effects attributable to the CeO_2 and Fe_2O_3 promoters, substantiating only a structural improvement favouring the exposure of active sites [53].

Although the reusability of MnO_x-based catalysts after washing and thermal regeneration treatments has been ascertained [14,20,22,29], Schurz et al. documented the occurrence of strong activity decay phenomena carrying out consecutive benzyl alcohol oxidation tests on amorphous MnO_2 and K-OMS-2 materials [27]. The marked activity loss of the M3C1 catalyst in the 2nd reaction cycle (Fig. 11), similar to that observed for all bare and promoted systems, confirms an unstable behaviour of MnO_x-based catalysts and the lack of steady-state conditions throughout the 1st reaction cycle. Hence, even if it is generally accepted that the oxidation of benzyl alcohol on MnO_x catalysts proceeds *via* the Mars–van Krevelen path, catalyst deactivation hinders any reliable assessment of reaction kinetics [22,27,54]. The mechanistic aspects of the

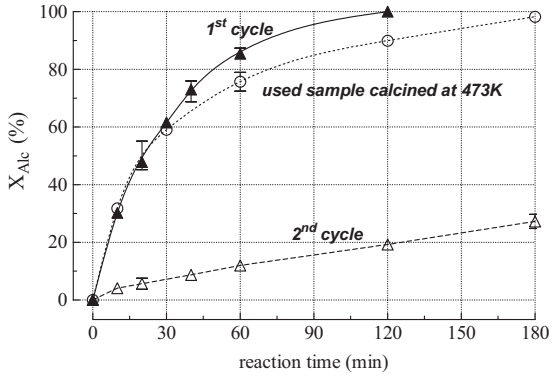

Fig. 11. Activity data of the M3C1 catalyst in the 1st and 2nd reaction cycles, and after calcination of the used sample (from 1st cycle) at 473 K.

activity–selectivity–stability pattern of bare and promoted MnO_x catalysts in the selective oxidation of benzyl alcohol will be fully addressed in a forthcoming study [54]; however, an almost full activity recovery after calcination of the used catalysts at $T \geq 473$ K (Fig. 11) indicates that the activity decay depends on the inhibition of active sites by slow rates of product(s) desorption and/or re-oxidation steps [27,54].

4. Conclusions

The effects of Ce and Fe addition on textural, structural and redox properties of MnO_x systems have been addressed.

The *redox-precipitation* synthesis route leads to *nanostructured* systems with much higher surface area and dispersion of the oxide phases promoting the catalyst reducibility.

Both the bare and promoted MnO_x systems drive the liquid-phase selective oxidation of benzyl alcohol to benzaldehyde ($S > 99\%$) with oxygen under mild conditions (323–363 K).

The dependence of the catalytic activity on the MnO_x loading and unchanging energy barrier values indicate the lack of electronic effects of Ce and Fe promoters on the functionality of the active phase.

Despite a loss in catalytic activity, catalyst regeneration following a soft calcination treatment ($T \geq 473$ K) has been ascertained.

References

[1] F. Bruhne, E. Wright, Benzaldehyde, Ullmann's Encyclopedia of Industrial Chemistry, Wiley-VCH, Weinheim, Germany, 2000.
[2] R.A. Sheldon, I. Arends, U. Hanefeld, Green Chemistry and Catalysis, Wiley-VCH Verlag GmbH & Co. KGaA, Weinheim, Germany, 2007.
[3] T. Mallat, A. Baiker, Chem. Rev. 104 (2004) 3037–3058.
[4] C. Parmeggiani, F. Cardona, Green Chem. 14 (2012) 547.
[5] K. Mori, K. Yamaguchi, T. Hara, T. Mizugaki, K. Ebitani, K. Kaneda, J. Am. Chem. Soc. 124 (2002) 11572–11573.
[6] T.L. Stuchinskaya, I.V. Kozhevnikov, Catal. Commun. 4 (2003) 417–422.
[7] C. Keresszegi, D. Ferri, T. Mallat, A. Baiker, J. Catal. 234 (2005) 64–75.
[8] N. Dimitratos, A. Villa, D. Wang, F. Porta, D. Su, L. Prati, J. Catal. 244 (2006) 113–121.
[9] M. Caravati, D.M. Meier, J.-D. Grunwaldt, A. Baiker, J. Catal. 240 (2006) 126–136.
[10] M. Caravati, J.-D. Grunwaldt, A. Baiker, Catal. Today 126 (2007) 27–36.
[11] V.R. Choudhary, R. Jha, P. Jana, Green Chem. 9 (2007) 267–272.
[12] X. Wang, H. Kawanami, S.E. Dapurkar, N.S. Venkataramanan, M. Chatterjee, T. Yokoyama, Y. Ikushima, Appl. Catal., A: Gen. 349 (2008) 86–90.
[13] C.Y. Ma, B.J. Dou, J.J. Li, J. Cheng, Q. Hu, Z.P. Hao, S.Z. Qiao, Appl. Catal., B: Environ. 92 (2009) 202–208.
[14] Y. Chen, H. Zheng, Z. Guo, C. Zhou, C. Wang, A. Borgna, Y. Yang, J. Catal. 283 (2011) 34–44.
[15] P.J. Miedziak, Q. He, J.K. Edwards, S.H. Taylor, D.W. Knight, B. Tarbit, C.J. Kiely, G.J. Hutchings, Catal. Today 163 (2011) 47–54.
[16] M.G. Buonomenna, E. Drioli, Appl. Catal., B: Environ. 79 (2008) 35–42.
[17] A. Dhakshinamoorthy, M. Alvaro, H. Garcia, D. Valencia, ACS Catal. 1 (2011) 48–53.
[18] M. Deng, G. Zhao, Q. Xue, L. Chen, Y. Lu, Appl. Catal., B: Environ. 99 (2010) 222–228.
[19] S. Higashimoto, N. Kitao, N. Yoshida, T. Sakura, M. Azuma, H. Ohue, Y. Sakata, J. Catal. 266 (2009) 279–285.
[20] Y. Son, V.D. Makwana, A.R. Howell, S.L. Suib, Angew. Chem. Int. Ed. 40 (2001) 4280–4283.
[21] H.-B. Ji, K. Ebitani, T. Mizugaki, K. Kaneda, Catal. Commun. 3 (2002) 511–517.
[22] V.D. Makwana, Y.-C. Son, A.R. Howell, S.L. Suib, J. Catal. 210 (2002) 46–52.
[23] H. Ji, K. Ebitani, T. Mizugaki, K. Kaneda, React. Kinet. Catal. Lett. 78 (2003) 73–80.
[24] V.R. Choudhary, D.K. Dumbre, V.S. Narkhede, S.K. Jana, Catal. Lett. 86 (2003) 229–233.
[25] Y. Su, L.-C. Wang, Y.-M. Liu, Y. Cao, H.-Y. He, K.-N. Fan, Catal. Commun. 8 (2007) 2181–2185.
[26] Q. Tang, T. Liu, Y. Yang, Catal. Commun. 9 (2008) 2570–2573.
[27] F. Schurz, J.M. Bauchert, T. Merker, T. Schleid, H. Hasse, R. Gläser, Appl. Catal., A: Gen. 355 (2009) 42–49.
[28] T. Sato, T. Komanoya, Catal. Commun. 10 (2009) 1095–1098.
[29] M. Ilyas, M. Saeed, Int. J. Chem. React. Eng. 9 (2011) A75.
[30] P. Paraskevopoulou, N. Psaroudakis, S. Koinis, P. Stavropoulos, K. Mertis, J. Mol. Catal. A: Chem. 240 (2005) 27–32.
[31] P.J. Figiel, A.M. Kirillov, Y.Y. Karabach, M.N. Kopylovich, A.J.L. Pombeiro, J. Mol. Catal., A: Chem. 305 (2009) 178–182.
[32] A.V. Biradar, M.K. Dongare, S.B. Umbarkar, Tetrahedron Lett. 50 (2009) 2885–2888.
[33] A. Jia, L.-L. Lou, C. Zhang, Y. Zhang, S. Liu, J. Mol. Catal., A: Chem. 306 (2009) 123–129.
[34] M.J. Beier, T.W. Hansen, J.-D. Grunwaldt, J. Catal. 266 (2009) 320–330.
[35] C. Zhu, L. Ji, Y. Wei, Catal. Commun. 11 (2010) 1017–1020.
[36] S. Bose, A. Pariyar, A.N. Biswas, P. Das, P. Bandyopadhyay, Catal. Commun. 12 (2011) 446–449.
[37] J.H.J. Kluytmans, A.P. Markusse, B.F.M. Kuster, G.B. Marin, J.C. Schouten, Catal. Today 57 (2000) 143–155.
[38] F. Arena, Catal. Sci. Technol. 4 (2014) 1890–1898.
[39] F. Arena, G. Trunfio, J. Negro, B. Fazio, L. Spadaro, Chem. Mater. 19 (2007) 2269–2276.
[40] F. Arena, G. Trunfio, J. Negro, L. Spadaro, Mater. Res. Bull. 43 (2008) 539–545.
[41] F. Arena, L. Spadaro, Nano-structured composite materials based on compositions of manganese and cerium, usable as oxidation catalysts and/or molecular adsorbers, WO 2012168957 (A1), 2012.
[42] H. Zou, Y.S. Lin, N. Rane, T. He, Ind. Eng. Chem. Res. 43 (2004) 3019–3025.
[43] M.F.L. Haris, C.-Y. Yin, Z.-T. Jiang, B.-M. Goh, X. Chen, W.a. Al-Masry, A.M. Abukhalaf, M. El-Harbawi, N.M. Huang, H.N. Lim, Ceram. Int. 40 (2014) 1245–1250.
[44] G. Qiu, H. Huang, S. Dharmarathna, E. Benbow, L. Sta, S.L. Suib, Chem. Mater. 23 (2011) 3892–3901.
[45] F. Arena, G. Trunfio, B. Fazio, J. Negro, L. Spadaro, J. Phys. Chem. C 113 (2009) 2822–2829.
[46] M. Fekete, R.K. Hocking, S.L.Y. Chang, C. Italiano, A.F. Patti, F. Arena, L. Spiccia, Energy Environ. Sci. 6 (2013) 2222.
[47] F. Arena, J. Negro, A. Parmaliana, L. Spadaro, G. Trunfio, Ind. Eng. Chem. Res. 46 (2007) 6724–6731.
[48] X. Shen, A.M. Morey, J. Liu, Y. Ding, J. Cai, J. Durand, Q. Wang, W. Wen, W.A. Hines, J.C. Hanson, J. Bai, A.I. Frenkel, W. Rei, M. Aindow, S.L. Suib, J. Phys. Chem. C 115 (2011) 21610–21619.
[49] F. Arena, T. Torre, C. Raimondo, A. Parmaliana, Phys. Chem. Chem. Phys. 3 (2001) 1911–1917.
[50] A. Bielanski, J. Haber, Oxygen in Catalysis, Marcel Dekker Inc., New York, NY, 1990.
[51] F. Arena, G. Trunfio, J. Negro, C. Saja, A. Raneri, L. Spadaro, Stud. Surf. Sci. Catal. 175 (2010) 493–496.
[52] T. Qinghu, W.U. Chengming, H. Xiaona, Y. Yanhui, Chin. J. Catal. 30 (2009) 207–212.
[53] X. Tang, J. Chen, X. Huang, Y. Xu, W. Shen, Appl. Catal., B: Environ. 81 (2008) 115–121.
[54] F. Arena, B. Gumina, A. Patti, C. Cannilla, L. Spadaro, L. Spiccia, Appl. Catal. B: Environ (2014), in preparation.